

## Article

# Octahedral Molybdenum Cluster-Based Nanomaterials for Potential Photodynamic Therapy

Marina Rodrigues Tavares <sup>1</sup>, Kaplan Kirakci <sup>2</sup>, Nikolay Kotov <sup>1</sup>, Michal Pechar <sup>1</sup>, Kamil Lang <sup>2</sup>, Robert Pola <sup>1,\*</sup> and Tomáš Etrych <sup>1</sup>

<sup>1</sup> Institute of Macromolecular Chemistry of the Czech Academy of Sciences, Heyrovského Náměstí 2, 162 06 Prague 6, Czech Republic

<sup>2</sup> Institute of Inorganic Chemistry of the Czech Academy of Sciences, 250 68 Husinec-Řež 1001, Czech Republic

\* Correspondence: pola@imc.cas.cz; Tel.: +420-296-809-216

**Abstract:** Photo/radiosensitizers, such as octahedral molybdenum clusters (Mo<sub>6</sub>), have been intensively studied for photodynamic applications to treat various diseases. However, their delivery to the desired target can be hampered by its limited solubility, low stability in physiological conditions, and inappropriate biodistribution, thus limiting the therapeutic effect and increasing the side effects of the therapy. To overcome such obstacles and to prepare photofunctional nanomaterials, we employed biocompatible and water-soluble copolymers based on *N*-(2-hydroxypropyl)methacrylamide (pHPMA) as carriers of Mo<sub>6</sub> clusters. Several strategies based on electrostatic, hydrophobic, or covalent interactions were employed for the formation of polymer-cluster constructs. Importantly, the luminescent properties of the Mo<sub>6</sub> clusters were preserved upon association with the polymers: all polymer-cluster constructs exhibited an effective quenching of their excited states, suggesting a production of singlet oxygen (O<sub>2</sub>(<sup>1</sup>Δ<sub>g</sub>)) species which is a major factor for a successful photodynamic treatment. Even though the colloidal stability of all polymer-cluster constructs was satisfactory in deionized water, the complexes prepared by electrostatic and hydrophobic interactions underwent severe aggregation in phosphate buffer saline (PBS) accompanied by the disruption of the cohesive forces between the cluster and polymer molecules. On the contrary, the conjugates prepared by covalent interactions notably displayed colloidal stability in PBS in addition to high luminescence quantum yields, suggesting that pHPMA is a suitable nanocarrier for molybdenum cluster-based photosensitizers intended for photodynamic applications.

**Keywords:** polymer carrier; photodynamic therapy; octahedral molybdenum clusters



**Citation:** Tavares, M.R.; Kirakci, K.; Kotov, N.; Pechar, M.; Lang, K.; Pola, R.; Etrych, T. Octahedral Molybdenum Cluster-Based Nanomaterials for Potential Photodynamic Therapy. *Nanomaterials* **2022**, *12*, 3350. <https://doi.org/10.3390/nano12193350>

Academic Editors: Fabien Grasset, Michael A. Shestopalov, Marta Feliz and Tetsuo Uchikoshi

Received: 19 August 2022

Accepted: 19 September 2022

Published: 26 September 2022

**Publisher's Note:** MDPI stays neutral with regard to jurisdictional claims in published maps and institutional affiliations.



**Copyright:** © 2022 by the authors. Licensee MDPI, Basel, Switzerland. This article is an open access article distributed under the terms and conditions of the Creative Commons Attribution (CC BY) license (<https://creativecommons.org/licenses/by/4.0/>).

## 1. Introduction

Photodynamic therapy (PDT) represents a very promising therapeutic modality which employs the light irradiation as external stimuli to activate compounds, so-called photosensitizers (PS), for the treatment of various malignant tumors. The crucial mechanism of this therapy is based on the interaction of a light-activated PS with molecular oxygen dissolved in the intracellular medium, thus producing reactive oxygen species, e.g., singlet oxygen, O<sub>2</sub>(<sup>1</sup>Δ<sub>g</sub>), which can damage critical cellular components. Their cytotoxicity affects cell's DNA, RNA, lipids, and proteins, resulting in tumor cell destruction. Selection of an appropriate PS is one of the most important factors influencing the efficacy of PDT. Various classes of compounds were described as PS for PDT, e.g., porphyrins, phthalocyanines, indocyanines, or bodipy dyes [1–3]. Nevertheless, the pharmacokinetics of PS plays a key role in the PDT treatment efficacy. Indeed, several research groups reported the encapsulation of numerous PS compounds to supramolecular systems, including polymer nanoparticles [4,5] and polymer micelles [4,6], and their controlled delivery. In particular, PS can be physically entrapped into nanoparticles by hydrophobic or electrostatic interactions of PS with biodegradable polymers, namely, poly(glycolic acid) [4,7], poly(lactic acid) [4,7], poly(lactic-co-glycolic acid) [8] and poly(ethylene glycol) [9].

Recently, octahedral molybdenum cluster compounds ( $\text{Mo}_6$ ) were reported as relevant photo/radiosensitizers for PDT [10–14], X-ray induced PDT [14–18], and photoinactivation of bacteria [11,19–22].  $\text{Mo}_6$  clusters are nanometer-sized metallic aggregates where the distances between the atoms are similar to those found in corresponding bulk metals, evidencing electron delocalization on the whole cluster. For stabilization, the clusters are surrounded by eight strongly bonded inner ligands ( $\text{L}^i$ ), generally halogen (Cl, Br, I), and six apical ligands ( $\text{L}^a$ ) that can be of either organic or inorganic nature to form a cluster denoted  $[\text{Mo}_6\text{L}^i_8\text{L}^a_6]^n$ . Upon excitation with UV, blue light, or X-rays, these complexes form long-lived triplet states that relax via a broad red-NIR luminescence. This emission is efficiently quenched by oxygen leading to the formation of  $\text{O}_2(^1\Delta_g)$  in high yields [23,24]. Even though a previous study showed the phototoxic activity of  $\text{Mo}_6$  complexes against the human cervical cancer cell line HeLa [25], their limited solubility and/or low stability in physiological conditions, as well as their lack of tumor selectivity, may result in a systemic toxicity, thus restricting their possible use in PDT [26].

To overcome these shortcomings, we hypothesized that the interaction of  $\text{Mo}_6$  with a suitable hydrophilic and biocompatible polymer carrier based on *N*-(2-hydroxypropyl)-methacrylamide (pHPMA) may improve both their stability in physiological conditions and also pharmacokinetic properties. The polymer conjugation may prolong half-life in circulation, significantly decrease interaction with serum proteins, promote a superior tumor specific accumulation, and reduce possible adverse effects, thus opening possibilities for their real clinical application. Previous studies have shown that PS molecules bound to pHPMA copolymers accumulate in the tumor via the enhanced permeability and retention (EPR) effect [1], in which the principle relies on the tumor tissues defective blood vessels and leaky vasculature combined with the poor lymphatic drainage, ensuring the  $\text{O}_2(^1\Delta_g)$  production in the tumor rather than in healthy tissues [2,27].

In this work, we describe the design, synthesis, and thorough evaluation of physico-chemical properties of HPMA-based polymer- $\text{Mo}_6$  constructs. We aimed to explore various strategies, such as covalent or non-covalent interactions, to bind  $\text{Mo}_6$  clusters to the polymer carriers and to optimize their structures for possible future applications in the field of polymer therapeutics, more specifically on tumor-targeted photodynamic therapy. In this study, the term “complexes” is employed for the non-covalent constructs based on electrostatic and hydrophobic interactions, while the term “conjugates” is used for the constructs prepared by the covalent azide-alkyne “click chemistry” (Figure 1). The relationship between the selected coupling strategy and properties of polymer- $\text{Mo}_6$  constructs is studied and described.

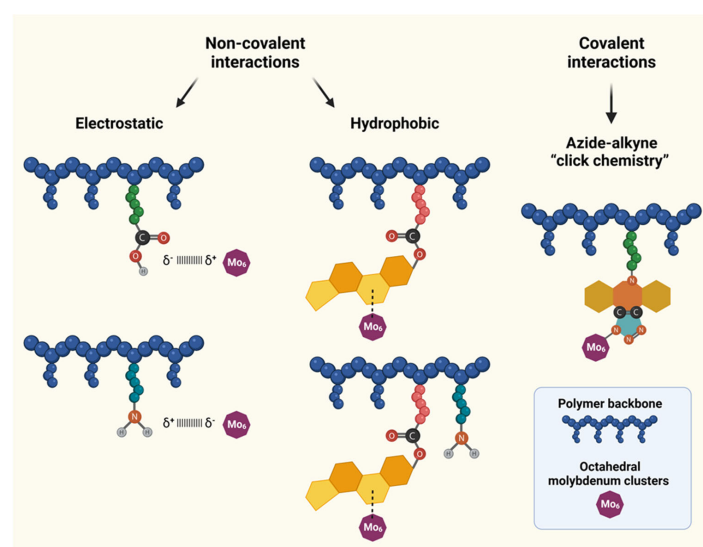


**Figure 1.** Schematic representation of non-covalent and covalent interaction approaches employed for binding of  $\text{Mo}_6$  clusters to polymer precursors;  $\text{Mo}_6$  cluster not-to-scale.

## 2. Materials and Methods

### 2.1. Materials

1,4-Dioxane, 2,2'-azobisisobutyronitrile (AIBN), 2-cyanopropan-2-yl dithiobenzoate (CTA-AIBN), 2-thiazoline-2-thiol, 2,4,6-trinitrobenzene-1-sulfonic acid (TNBSA), 3-azido-1-propylamine, 4,4'-azobis(4-cyanopentanoic acid) (ACVA), 4-cyano-4-(thiobenzoylthio)-pentanoic acid (CTA-ACVA), dimethyl sulfoxide (DMSO), methacryloyl chloride, *N,N*-diisopropylethylamine (DIPEA), *N,N*-dimethylacetamide (DMA), phosphate buffered saline (phosphate buffer 0.01M and NaCl 0.154M, pH 7.4) (PBS), and *t*-butanol were purchased from Sigma-Aldrich (Prague, Czech Republic). 2,2'-Azobis(4-methoxy-2,4-dimethylvaleronitrile) (V-70) was from Fujifilm Wako Chemicals Europe (Neuss, Germany). 3-Amino-1-(11,12-didehydrodibenzo[b,f]azocin-5(6H)-yl)propan-1-one (DBCO-NH<sub>2</sub>) was from Click Chemistry Tools (Scottsdale, AZ, USA). *N*-(3-*tert*-butoxycarbonylaminopropyl)methacrylamide (APMA-Boc) was purchased from Polysciences, Inc. (Warrington, PA, USA), and 1-aminopropan-2-ol was from TCI Europe (Zwijndrecht, Belgium). All solvents and chemicals were of analytical grade.

### 2.2. Synthesis of Monomers

The monomers HPMA [28], 3-methacrylamidopropanoylthiazolidine-2-thione (MA-AP-TT) [29] and cholest-5en-3 $\beta$ -yl 6-methacrylamido hexanoate (MA-AH-cholesterol) [30] were prepared according to the literature. High Performance Liquid Chromatography (HPLC) analysis was employed to verify the purity of monomers and chain transfer agents. Analysis was performed using a Shimadzu HPLC system with a C18 reversed-phase Chromolith Performance RP-18e column and a diode array detector (Shimadzu SPD-M20A), using water/acetonitrile (gradient of 5–95% *v/v* acetonitrile) as eluent with 5 mL min<sup>-1</sup> flow rate.

### 2.3. Synthesis of Polymer Precursors P1–P5

Statistical copolymers were prepared by reversible addition–fragmentation chain transfer (RAFT) polymerization of HPMA with respective monomers as follows: MA-AP-TT was employed for **P0a**, **P0b**, **P1**, and **P5** copolymers; APMA-Boc for **P2** [31]; MA-AH-cholesterol for **P3**; MA-AH-cholesterol and APMA-Boc for **P4**. The chain transfer agent CTA-AIBN was used for all precursors except for **P2**, in which CTA-ACVA was employed instead. Reaction conditions were adapted from our previous studies [32], using a mixture of *t*-butanol and DMA for all precursors except for **P2**, in which a mixture of water and dioxane was employed. Dithiobenzoate (DTB) groups originating from CTA were removed by reaction with an excess of AIBN as previously described [33]. For **P2** and **P4**, *t*-butoxycarbonyl (Boc) groups were removed by heating in distilled water at 150 °C for 1 h [34]. Copolymer **P1** with COOH groups along the polymer chain was prepared via hydrolysis of thiazolidine-2-thione (TT) groups of the polymer precursor poly(HPMA-*co*-MA-AP-TT) in phosphate buffer (pH 8.0). Detailed structures of copolymer precursors **P1–P5** are shown in Figure 2, and their physico-chemical characterization is described in Table 1. Detailed synthetic procedures and the ratio between monomers, chain transfer agents, and initiators are described in Supplementary Materials. <sup>1</sup>H NMR spectra of polymer precursors **P3** and **P4** are shown in Supplementary Materials.

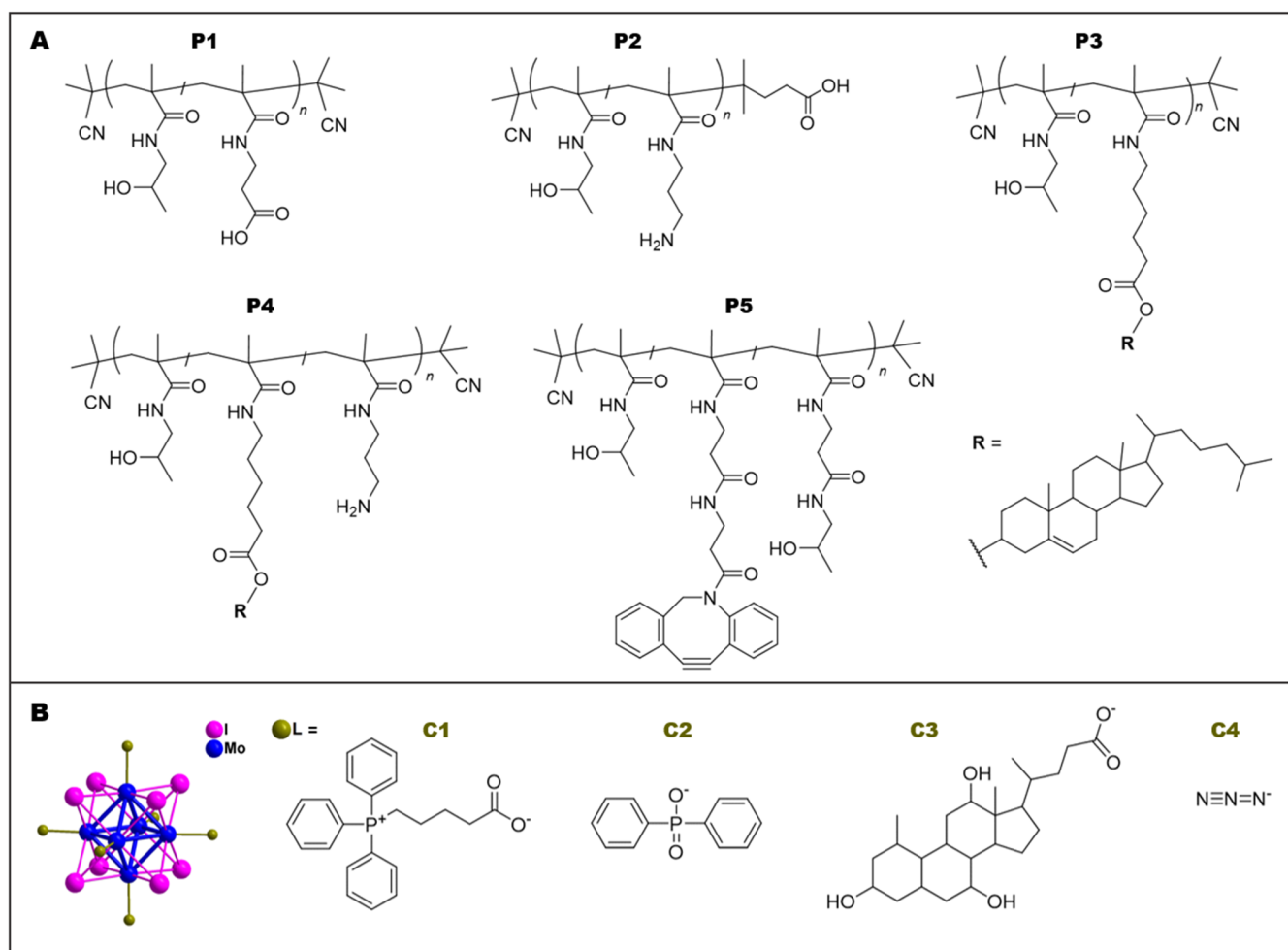


**Figure 2.** Polymer precursors and Mo<sub>6</sub> clusters used for non-covalent and covalent interactions: (A) chemical structures of precursors P1–P5; (B) schematic representation of the molecular structure of [Mo<sub>6</sub>L<sup>i</sup><sub>8</sub>L<sup>a</sup><sub>6</sub>]<sup>n</sup> cluster and ligands for clusters C1–C4; color coding: molybdenum (blue), iodine (L<sup>i</sup>: magenta), apical ligands (L<sup>a</sup>: green); hydrogen atoms are omitted for clarity.

**Table 1.** Physico-chemical characteristics of the polymer precursors.

Polymer Precursor	Structure	Functional Group	Functional Groups (mol. %) <sup>a</sup>	M <sub>w</sub> (g/mol) <sup>b</sup>	Đ <sup>b</sup>	D <sub>H</sub> (nm) <sup>c</sup>
P0a	poly(HPMA-co-MA-AP-TT)	TT	(a) 1.9	18,500	1.03	5.9 ± 0.7
P0b	poly(HPMA-co-MA-AP-TT)	TT	(b) 10.2	39,200	1.04	7.4 ± 0.4
P1	poly(HPMA-co-MA-AP-COOH)	COOH	1.9	18,700	1.05	5.3 ± 0.2
P2	poly(HPMA-co-APMA)	NH <sub>2</sub>	5.1	24,100	1.04	4.9 ± 0.1
P3	poly(HPMA-co-MA-Acap-cholesterol)	cholesterol	2.3	26,400	1.06	39.9 ± 1.1
P4	poly(HPMA-co-APMA-co-MA-AH-cholesterol)	cholesterol + NH <sub>2</sub>	2.5 cholesterol 2.3 NH <sub>2</sub>	24,600	1.07	26.8 ± 0.7
P5	poly(HPMA-co-MA-AP-DBCO)	DBCO	8	40,000	1.06	11.5 ± 0.8

<sup>a</sup> Contents of TT, DBCO, and NH<sub>2</sub> groups were evaluated by UV–VIS spectrophotometry; the content of cholesterol was determined using NMR Spectroscopy. <sup>b</sup> The weight-average molecular weight (M<sub>w</sub>) and dispersity (Đ) were determined using SEC with RI and MALS detection. The analysis was performed using a TSK 3000 SWXL column with methanol/0.3 M sodium acetate buffer, pH 6.5 (4/1, v/v), as a mobile phase. <sup>c</sup> The mean hydrodynamic diameter (D<sub>H</sub>) was obtained by DLS with intensity of scattered light detected at angle θ = 173° in PBS.

#### 2.4. Synthesis of Mo<sub>6</sub> Clusters C1–C4

Previously published procedures were employed to prepare Mo<sub>6</sub> cluster compounds: [Mo<sub>6</sub>I<sub>8</sub>(OCOC<sub>4</sub>H<sub>8</sub>PPh<sub>3</sub>)<sub>6</sub>]Br<sub>4</sub> (**C1**) [12], Na<sub>2</sub>[Mo<sub>6</sub>I<sub>8</sub>(OPOPh<sub>2</sub>)<sub>6</sub>] (**C2**) [11], Na<sub>2</sub>[Mo<sub>6</sub>I<sub>8</sub>(cholate)<sub>6</sub>] (**C3**) [35], and Na<sub>2</sub>[Mo<sub>6</sub>I<sub>8</sub>(N<sub>3</sub>)<sub>6</sub>] (**C4**) [36]. Schematic structures of clusters **C1–C4** are shown in Figure 2. For characterization see Table 2.

**Table 2.** Physico-chemical characteristics of Mo<sub>6</sub> clusters.

Cluster	Formula	M <sub>w</sub> (g/mol)	D <sub>H</sub> (nm) <sup>a</sup>	ZP (mV) <sup>a</sup>	Charge
<b>C1</b>	[Mo <sub>6</sub> I <sub>8</sub> (OCOC <sub>4</sub> H <sub>8</sub> PPh <sub>3</sub> ) <sub>6</sub> ]Br <sub>4</sub>	4084.9	48.4 ± 5.3	13	4
<b>C2</b>	Na <sub>2</sub> [Mo <sub>6</sub> I <sub>8</sub> (OPOPh <sub>2</sub> ) <sub>6</sub> ]	2939.9	20.2 ± 11.6	−67	−2
<b>C3</b>	Na <sub>2</sub> [Mo <sub>6</sub> I <sub>8</sub> (cholate) <sub>6</sub> ]	4082.0	5.9 ± 1.4	−9	−2
<b>C4</b>	Na <sub>2</sub> [Mo <sub>6</sub> I <sub>8</sub> (N <sub>3</sub> ) <sub>6</sub> ]	1889.0	60.6 ± 15.3	−16	−2

<sup>a</sup> The mean hydrodynamic diameter (D<sub>H</sub>) and zeta potential (ZP) were obtained by DLS measurement with intensity of scattered light detected at angle θ = 173° in deionized water (pH ~ 6).

#### 2.5. Synthesis of Polymer-Cluster Constructs POL1–POL6

Different conjugation strategies were exploited aiming to optimize the constructs' structure for possible future applications in the field of polymer therapeutics. In this study, the term “complexes” is employed for the non-covalent constructs based on electrostatic (**POL1–POL2**) and hydrophobic (**POL3–POL4**) interactions, while the term “conjugates” is used for the constructs using covalent attachment of the Mo<sub>6</sub> clusters to the polymer backbone (**POL5–POL6**). The physico-chemical characterization of polymer-cluster constructs **POL1–POL6** is shown in Table 3, and their detailed synthetic procedures are described below.

**Table 3.** Physico-chemical and photophysical characteristics of polymer-cluster constructs.

Polymer-Cluster Constructs	Prepared From	Type of Interaction	Mo Cluster (wt%)	D <sub>H</sub> (nm) <sup>a</sup>	ZP (mV) <sup>a</sup>	λ <sub>L</sub> (nm) <sup>b</sup>	Φ <sub>L</sub> (Ar) <sup>b</sup>	Φ <sub>L</sub> (air) <sup>b</sup>	F <sub>T</sub> (air) <sup>b</sup>
<b>POL1</b>	P1 + C1	Electrostatic	11.5	5.1 ± 1.1	9	695	0.16	0.04	0.75
<b>POL2</b>	P2 + C2	Electrostatic	25.9	29.2 ± 9.0	4	690	0.39	0.08	0.79
<b>POL3</b>	P3 + C3	Hydrophobic	20.0	8.4 ± 2.3	−14	690	0.25	0.05	0.80
<b>POL4</b>	P4 + C3	Hydrophobic	20.0	12.0 ± 3.1	1	695	0.49	0.09	0.82
<b>POL5</b>	P5 + C4	Covalent	14.2	7.3 ± 1.1	−17	685	0.25	0.06	0.76
<b>POL6</b>	P5 + C4 + azide-NH <sub>2</sub>	Covalent	14.2	11.0 ± 0.9	−7	685	0.25	0.06	0.76

<sup>a</sup> The mean hydrodynamic diameter (D<sub>H</sub>) and zeta potential (ZP) were obtained by DLS with intensity of scattered light detected at angle θ = 173° in deionized water (pH ~ 6). <sup>b</sup> λ<sub>L</sub> is the maximum of luminescence emission bands; Φ<sub>L</sub>(Ar) and Φ<sub>L</sub>(air) are the luminescence quantum yields in argon- and air-saturated dispersions, respectively (excitation wavelength was 400 nm); F<sub>T</sub>(air) is the fraction of the triplet states quenched by oxygen in air saturated solutions: F<sub>T</sub>(air) = 1 − Φ<sub>L</sub>(air)/Φ<sub>L</sub>(Ar).

##### 2.5.1. Electrostatic Non-Covalent–POL1 and POL2

Solutions of the polymer precursor and the cluster, each in 100 μL of methanol, were prepared separately. In case of cluster solution, addition of 10 μL of DMSO was necessary for complete dissolution. Aliquots of 50 μL from each solution were mixed together and vortexed for 10 min. The reaction mixture was added into 1 mL of distilled water and kept under stirring at room temperature for 1 h. Then, methanol was removed under vacuum, and water was added to adjust the volume to 1 mL. The resulting solutions were used for dynamic light scattering (DLS) and quantum yield (QY) measurements. **POL1** was composed of **P1** (10 mg, 1.3 μmol of -COOH) and cluster **C1** (1.3 mg, 0.32 μmol) while **POL2** was composed of **P2** (10 mg, 2.35 μmol of -NH<sub>2</sub>) and cluster **C2** (3.5 mg, 1.19 μmol).

### 2.5.2. Hydrophobic Non-Covalent Complexes–POL3 and POL4

The procedure for preparation of **POL3** and **POL4** was analogous to the one described in 2.5.1., except that the addition of DMSO was not necessary for dissolution of the cluster **C3**. **POL3** was composed of **P3** (10 mg) and cluster **C3** (2.5 mg) while **POL4** was composed of **P4** (10 mg) and cluster **C3** (2.5 mg).

### 2.5.3. Covalent Conjugates–POL5–POL6

A solution of **P5** (300 mg, 145  $\mu\text{mol}$  of DBCO groups) in dry methanol (2.4 mL) was added into a solution of cluster **C4** (49.6 mg, 145  $\mu\text{mol}$  of azide groups) in 0.75 mL of dry methanol under stirring. The reaction mixture was maintained under argon for 30 min; then, it was stirred at 25 °C overnight. Isolation and purification procedures were performed as follows: first, the polymer was precipitated into a mixture of acetone/diethyl ether (1/1) twice. The product was washed with pure diethyl ether and dried under vacuum, affording the polymer-cluster conjugate **POL5** (296 mg, 93%). HPLC analysis was performed to control the course of reactions. **POL6** was prepared analogously to **POL5**; however, part of DBCO groups was reacted with 3-azido-1-propylamine via a copper-free alkyne-azide cycloaddition as follows: 3-azido-1-propylamine (1.3  $\mu\text{L}$ , 13.6  $\mu\text{mol}$ ) was added to a solution of **P5** (150 mg, 72.5  $\mu\text{mol}$  of DBCO groups) in dry DMA (2 mL) followed by cluster **C4** (49.6 mg, 145  $\mu\text{mol}$  of azide groups) in 0.75 mL of dry methanol. The reaction mixture was bubbled with argon; then, it was stirred for 3 h at 24 °C. The reaction mixture was diluted with methanol (2 mL) and purified using a Sephadex LH-20 column with methanol elution and UV detection. The conjugate-containing fraction was collected and concentrated under vacuum to 2 mL. The polymer was isolated by precipitation into the mixture of acetone and diethyl ether (2/1; 100 mL) and dried to yield **POL6** (136 mg; yield 91%).

## 2.6. Physico-Chemical and Photophysical Characterization

### 2.6.1. Size Exclusion Chromatography (SEC)

The number-average molecular weight ( $M_n$ ), weight-average molecular weight ( $M_w$ ), and dispersity ( $\mathcal{D}$ ) of polymer precursors **P1–P5** and polymer-cluster conjugates **POL5** and **POL6** were determined by a Shimadzu HPLC system equipped with a size exclusion chromatography (SEC) column TSK 3000 SWXL column (Tosoh Bioscience, Tokyo, Japan). Evaluation was carried out using a multi-angle light scattering (MALS) DAWN HELEOS II (Wyatt Technology Co., Santa Barbara, CA, USA), photodiode array SPD-M20A (Shimadzu, Japan) and differential refractometer index Optilab<sup>®</sup>-rEX (Wyatt Technology Co., Santa Barbara, CA, USA) detectors. The analysis was performed using a mixture of methanol and 0.3 M sodium acetate buffer, pH 6.5 (4/1, *v/v*) as a mobile phase at a flow rate of 0.5 mL min<sup>-1</sup>. The ASTRA software (version 8.1, Wyatt Technology Co., Santa Barbara, CA, USA) was used for calculation of  $M_w$  and  $\mathcal{D}$  values.

### 2.6.2. Dynamic Light Scattering (DLS)

The hydrodynamic diameter ( $D_h$ ) and surface zeta potential (ZP) of all samples was measured using a Nano-ZS instrument (ZEN3600, Malvern, UK) with a laser wavelength of 632.8 nm, and the intensity of the scattered light was detected at an angle  $\theta = 173^\circ$ . Precursors were dissolved in PBS at 1 mg mL<sup>-1</sup>. Clusters and polymer-cluster constructs were dissolved in methanol, and aliquots of these solutions were added to deionized water (pH~6) or PBS to obtain the final concentration of 1 mg mL<sup>-1</sup>; their long-term stability was evaluated. The values were determined as a mean of at least five independent measurements.

### 2.6.3. UV–VIS Spectrophotometry

UV–VIS spectrophotometry (Specord 205 ST, Analytic Jena AG, Jena, Germany) was used for determination of the content of TT, DBCO, and amine groups. The molar absorption coefficient of  $\epsilon(\text{TT}) = 10,300 \text{ L mol}^{-1} \text{ cm}^{-1}$  ( $\lambda_{\text{max}} = 305 \text{ nm}$ ) in methanol was used for determination of TT groups in the polymer precursors before hydrolysis (**P1**) or aminolysis

(P5). In the case of DBCO groups,  $\epsilon(\text{DBCO}) = 13,000 \text{ L mol}^{-1} \text{ cm}^{-1}$  ( $\lambda_{\text{max}} = 292 \text{ nm}$ ) in methanol was employed. The content of amine groups in polymer precursors **P2**, **P4**, and polymer-cluster conjugate **POL6** was determined using a modified TNBSA assay as published earlier [37]. For **P2** and **POL6**, the solution was prepared in borate buffer (0.1 M  $\text{Na}_2\text{B}_4\text{O}_7 \cdot 10\text{H}_2\text{O}$ , pH 9.3) at the concentration of  $2 \text{ mg mL}^{-1}$ . An aliquot of  $100 \mu\text{L}$  of this solution was mixed with borate buffer ( $875 \mu\text{L}$ ) and 0.03 M solution of TNBSA in water ( $25 \mu\text{L}$ ). The molar absorption coefficient  $\epsilon(\text{NH}_2) = 17,200 \text{ L mol}^{-1} \text{ cm}^{-1}$  ( $\lambda_{\text{max}} = 500 \text{ nm}$ ) was used, and the absorbance was measured after 90 min of incubation. In the case of **P4**, a similar evaluation method was employed, but the sample was dissolved in a mixture of borate buffer and DMSO (9/1) due to the hydrophobic character of cholesterol moieties [30].

#### 2.6.4. Nuclear Magnetic Resonance (NMR) Spectroscopy

For determination of cholesterol content in polymer precursors **P3** and **P4**,  $^1\text{H}$  NMR spectra were measured with a Bruker Avance III 600 spectrometer (Bruker, Karlsruhe, Germany) operating at 600.2 MHz using  $\text{DMSO-}d_6$  as solvent. Typical conditions for measurements of the spectra were as follows:  $\pi/2$  pulse width  $10 \mu\text{s}$ , relaxation delay  $10 \text{ s}$ , spectral width  $10 \text{ kHz}$ , acquisition time  $3.21 \text{ s}$ , 200 scans, and 5 mm NMR tubes were used. The content of cholesterol moieties statistically distributed along the polymer backbone was assessed using the integral intensities of signals at  $\delta \approx 4.71 \text{ ppm}$  (1 H, OH) and  $\delta \approx 3.67 \text{ ppm}$  (1 H, CH) from the HPMA monomer unit and the integral intensity of the signal at  $\delta \approx 5.34 \text{ ppm}$  (1 H, CH) from C-6 of cholesterol moiety. NMR data for both polymer precursors are shown in the Supplementary Materials, Section S2.

#### 2.6.5. Attenuated Total Reflectance (ATR) Fourier-Transform Infrared (FTIR) Spectroscopy

ATR FTIR spectra were recorded using a Thermo Nicolet Nexus 870 FTIR spectrometer (Bruker, Karlsruhe, Germany) purged with dry air and equipped with a liquid-nitrogen-cooled MCT (mercury cadmium telluride) detector. All the spectra were acquired using a Golden Gate single reflection ATR accessory (Specac Ltd., Orpington, UK) equipped with a diamond internal reflection element. Measurements were performed at room temperature using the following parameters: resolution  $4 \text{ cm}^{-1}$  and 256 scans. All data were processed in the OMNIC software (ver. 8.3.103). The atmosphere spectrum was subtracted from the acquired spectra, and then, the resulting spectra were subjected to the baseline and ATR corrections. Measurements were performed for solutions of **C4**, **POL5**, and **POL6** in distilled water at 0.2 wt. % of  $\text{Mo}_6$ -cluster equivalent.

#### 2.6.6. Luminescence Spectroscopy

Absolute photoluminescence quantum yields and emission spectra in deionized water or PBS were measured using a Quantaurus QY C11347-1 spectrometer (Hamamatsu, Japan). The samples were prepared by adding small aliquots of concentrated methanol solutions of the polymer-cluster constructs to deionized water or PBS to reach the final concentration of  $0.1 \text{ mg mL}^{-1}$ . All samples were excited at 400 nm. In order to perform measurements under various concentrations of dissolved oxygen, the aqueous solutions of the clusters and the corresponding polymer constructs were saturated with air or argon.

### 3. Results and Discussion

In order to prevent  $\text{Mo}_6$  clusters' aggregation in aqueous solutions, we present novel synthetic strategies for the synthesis of biocompatible polymer-coated  $\text{Mo}_6$  cluster constructs by employing covalent or non-covalent interactions with various pHPMA copolymers differing in their structure. This study is focused on the physico-chemical and photophysical properties of the polymer-cluster constructs intended as nanomedicines for anti-tumor therapy.

### 3.1. Synthesis of Polymer Precursors

Controlled RAFT polymerization technique was employed in order to prepare well-defined polymer precursors with an appropriate number of functional groups, such as TT, COOH, NH<sub>2</sub>, and DBCO moieties, which are used for further chemical modifications.

First, poly(HPMA-*co*-MA-AP-TT) (**P0a**) containing reactive TT groups were prepared and subsequently hydrolyzed in phosphate buffer (pH 8.0) to yield poly(HPMA-*co*-MA-AP-COOH) (**P1**). Even though much higher amounts of negatively charged groups may be necessary for stronger electrostatic interactions between the polymer and molybdenum molecule, highly, negatively charged systems tend to be captured by the reticuloendothelial system (RES), mainly in the liver and spleen, thus impairing their use for in vivo applications [38]. Therefore, a lower ratio of MA-AP-TT related to HPMA was used for the polymerization of **P0a** precursor, resulting in copolymers with 1.9 mol. % of final reactive groups and  $M_w \approx 18,700 \text{ g} \cdot \text{mol}^{-1}$ .

Another poly(HPMA-*co*-MA-AP-TT) (**P0b**) was prepared, but using a higher ratio of MA-AP-TT related to HPMA, as well as a higher amount of monomers related to CTA and initiator in the reaction mixture, resulting in a precursor containing 10.2 mol. % of reactive TT groups and  $M_w \approx 39,200 \text{ g} \cdot \text{mol}^{-1}$ . Here, the respective content of functional groups was chosen aiming to afford a precursor with a higher number of moieties available for further covalent interactions. To prepare **P5** containing 8 mol. % of DBCO groups, **P0b** was reacted with an amine-functionalized DBCO. The copper-free click chemistry approach was selected to avoid the use of copper in further reactions, thus reducing toxicity-related risks and also avoiding time-consuming and complicated purification steps [39].

Higher amounts of positively charged groups on polymer precursors may be necessary to achieve stronger electrostatic interactions with negatively charged molybdenum clusters. Unfortunately, a higher content of amine groups is known to generate toxicity in vitro and in vivo; therefore, the ratio of comonomers was optimized to afford poly(HPMA-*co*-APMA-Boc) (**P2**) containing approximately 5.5 mol. % of amine groups.

The introduction of hydrophobic moieties, such as cholesterol or its derivatives, into the structure of the water-soluble polymer carrier switches the character of the polymers to their amphiphilic nature [30,40–42]. Such amphiphilic polymers can either self-assemble into the core-shell micellar structures or can form a coating of hydrophobic nanoparticles or liposomes via interaction of cholesterol moiety with hydrophobic compartments of those nanomaterials [43,44]. According to the described procedures [30,40], the amphiphilic polymer precursors **P3** and **P4** were prepared containing 2.3 and 2.5 mol. % of cholesterol moieties, respectively, and comparable molecular weights around  $25,000 \text{ g} \cdot \text{mol}^{-1}$  with narrow dispersity. For <sup>1</sup>H-NMR spectra of **P3** and **P4**, see Figures S1 and S2, respectively. The introduction of certain number of amine groups into the polymer precursor **P4** was performed to adjust the negative charge of C3, thus improving the properties of the system for eventual in vivo applications. According to the published data, neutral nanomedicines exhibit more favorable pharmacokinetic properties such as plasma half-life, recognition by RES, and possible adhesion to vascular endothelium [38].

Linear precursors **P1** and **P2** exhibited hydrodynamic diameters in aqueous solution around 5 nm, typical for HPMA-based polymer random coils, whereas the diameter of **P5** was significantly higher ( $D_H \approx 11 \text{ nm}$ ) indicating eventual association of the macromolecules due to the presence of the hydrophobic pendant DBCO group and a higher molecular weight of the polymers. As expected, **P3** showed the highest hydrodynamic diameter ( $D_H \approx 40 \text{ nm}$ ) due to the hydrophobic characteristic of pendant cholesterol moieties, which enable **P3** to form micelles in aqueous solution, as already observed in our previous studies of such HPMA copolymers with cholesterol derivatives [40,41]. Nevertheless, positively charged amine moieties distributed along the same polymer backbone (**P4**) may have contributed to the formation of smaller micelles ( $D_H \approx 27 \text{ nm}$ ), probably due to the increased hydrophilicity of the precursor, hence impairing the formation of larger micelles.

Detailed structures and physico-chemical characterization of the polymer precursors **P1**–**P5** are shown in Figure 2 and Table 1, respectively.

### 3.2. Preparation of Polymer-Cluster Constructs

In this study, several conjugation strategies were exploited aiming to optimize the constructs' structure for possible future applications in the field of polymer therapeutics. Our initial attempts relied on the use of non-covalent electrostatic and hydrophobic interactions for preparation of the non-covalent constructs (**POL1–POL2**) and (**POL3–POL4**), respectively, which are referred to as “complexes”. Afterwards, the covalent attachment of the  $\text{Mo}_6$  clusters was employed to prepare **POL5–POL6**, which are called by the term “conjugates”.

The structures of precursors **P1–P4** and clusters **C1–C3**, used for non-covalent complex formation, and precursor **P5** and cluster **C4**, used for preparation of the covalent conjugates, are summarized in Figure 2.

Polymer-cluster complexes **POL1** and **POL2** were prepared by employing electrostatic interactions between **P1** and **P2** with the positively and negatively charged  $\text{Mo}_6$  clusters **C1** and **C2**, respectively. An equimolar ratio between the oppositely charged functional groups of the polymer precursors and clusters was used. Consequently, this resulted in various contents of the clusters within their respective complexes: **POL1** (11.5 wt%, cluster charge 4+) and **POL2** (25.9 wt%, cluster charge 2–). **POL1** exhibited ZP value +9 mV which was slightly lower than that of cluster **C1** (+13 mV) as a consequence of the electrostatic complex formation with the negatively charged polymer precursor **P1**. Although the change in ZP value was relatively low, the formation of the complex **POL1** was accompanied with a dramatic change of the hydrodynamic diameter from 48 nm of the cluster **C1** (that tends to aggregate in water) to 5 nm of the polymer-coated complex **POL1**. The cluster–polymer interaction in this particular case enabled to obtain the unimolecular complexes presented in single cluster molecules coated by the hydrophilic copolymer. Most probably, the cluster containing +4 charge is coated with one or two polymer chains affording a slightly positive complex and a small dimension in contrast to huge aggregates of **C1** cluster molecules. When the polymer precursor **P2** with amine groups was employed for the complex formation, a significant increase in the zeta potential of complex **POL2** (+4 mV), reaching almost neutral complex, was observed in comparison to the highly negatively charged cluster **C2** (–67 mV) used in complexation. Such behavior indicate that the cluster was successfully modified with the positively charged polymer. Importantly, the hydrodynamic size of complex **POL2** was significantly higher ( $D_h \approx 30$  nm) compared with **POL1** ( $D_h \approx 5$  nm). We hypothesize that this was caused by the presence of much higher content of amino groups on polymer than the carboxyl groups on the cluster. The polymer coated sufficiently the clusters, but one polymer chain was generally involved in the coating of more than one cluster molecule in solution, thus the crosslinking of the polymer-cluster **C2** occurred and increased the size.

Another non-covalent method of the polymer-cluster complex preparation explored in this study was based on hydrophobic interactions of polymer precursors **P3** and **P4**, both bearing hydrophobic cholesterol moieties, with the cholate-based cluster **C3**, affording the polymer-cluster complexes **POL3** and **POL4**, respectively. Loading of 20 wt. % of  $\text{Mo}_6$  cluster was chosen for both complexes **POL3** and **POL4**. The introduction of amine groups to polymer **P4** was performed to verify the influence of the positive charge upon the formation of the hydrophobic complexes (**POL3** and **POL4**). After interaction of precursor **P3**, bearing cholesterol moieties and neutral charge, with **C3** (ZP = –9 mV), the zeta potential of the resulting complex **POL3** slightly dropped to –14 mV. Opposite to that, a neutral to slightly positive surface charge (+1 mV) was observed when amine groups were introduced into the structure of **POL4**, showing the benefit caused by the addition of amino groups to the complex. The hydrodynamic sizes of original **P3** and **P4** polymers,  $D_h \approx 40$  and 27 nm, respectively, showed formation of the micelles self-assembled from these amphiphilic copolymers. Importantly, after the complexation with **C3**, both complexes **POL3** and **POL4** showed smaller hydrodynamic sizes,  $D_h = 8.4$  and 12 nm, respectively, in comparison to their polymer precursors. We summarize that the observed change in size upon the addition of the hydrophobic moieties containing cluster is most probably caused by disruption of the self-assembled micellar vesicles formed by the amphiphilic

polymer precursors and subsequent rearrangement of the polymer chains around the hydrophobic cluster in aqueous solution. In contrast to **POL2** and similarly to **POL1**, both **POL3** and **POL4** are rather formed by a single molecule of cluster coated by a small number of polymer chains. Physico-chemical characteristics of Mo<sub>6</sub> clusters are shown in Table 2.

With respect to the limited colloidal stability of the non-covalent polymer-cluster complexes, which will be further discussed within this manuscript, we evaluated the covalent binding of Mo<sub>6</sub> clusters to the polymer carriers as an alternative approach. For this purpose, DBCO groups from polymer precursor **P5** were used for the attachment of Mo<sub>6</sub> cluster **C4** via a copper-free alkyne-azide cycloaddition (“click reaction”), affording stable covalent polymer-cluster conjugates **POL5** and **POL6**. For both conjugates, the content of Mo<sub>6</sub> cluster was calculated considering the ratio 1/1 between DBCO groups on polymer precursor and azide groups on cluster moiety.

It is generally known that the highly positively charged systems should be toxic for the body cells and can adhere to the negative vascular endothelium, leading to a lower concentration in the plasma along with an impaired EPR effect [38]. On the other hand, highly negatively charged systems are easily recognized taken up by the immune system, and then stacked in the kidneys. To avoid such effects and potential drawbacks, the ideal surface charge should be neutral or only slightly negative. Therefore, additional amine groups were introduced into the polymer-cluster conjugate **POL6** via reaction of the conjugate **POL5** with 3-azido-1-propylamine to neutralize the negative charge on the cluster and make the conjugate neutral in charge.

Infrared spectroscopy was used to measure the conversion of the alkyne-azide cycloaddition. The efficiency of **C4** conjugation to **P5** was determined using the strong asymmetric stretching vibration mode of azide groups [45–47]. To assess the amount of unreacted azide groups, a reference was set up as the integral area of the asymmetric stretching vibrational band of azide groups centered at 2056 cm<sup>-1</sup> of **C4** (0.2 wt% Mo<sub>6</sub>-cluster in distilled water; Figure 3, dark grey line) [45,46]. This typical complex profile can be attributed to weak Fermi resonance of the vibration with combination tones of C–N stretching vibrations and partly to possible differences in local environments of the six azide groups [47,48]. The azide band’s shift to a lower wavenumber (2056 cm<sup>-1</sup>) compared to the typical position described in the literature was attributed to the presence of charged molybdenum and iodine atoms in the cluster’s structure [47]. Additionally, the cluster forms a stable colloid in water, and azide groups are involved in H-bonding with water molecules [48] which may contribute to the observed red-shifted position of the band.

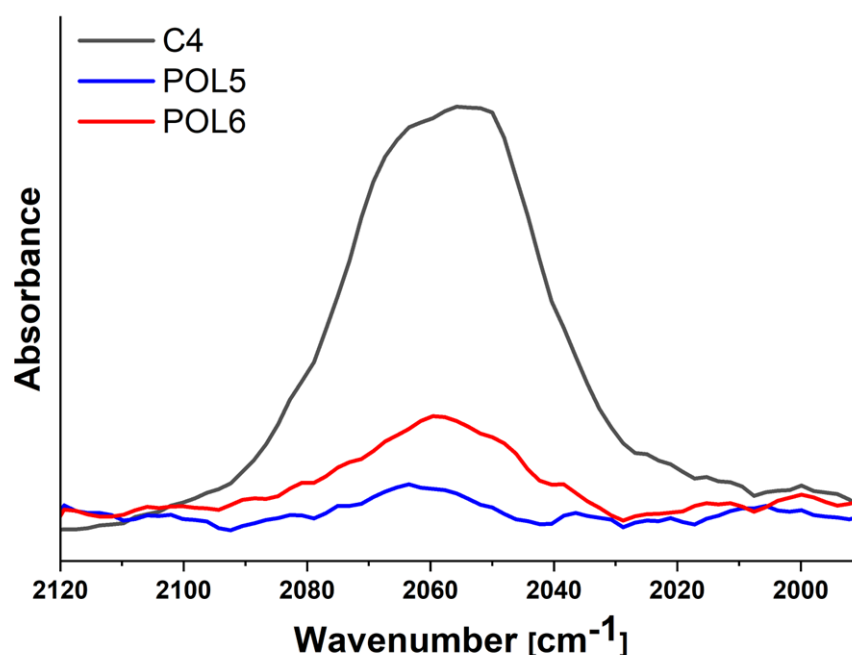


**Figure 3.** The region of stretching vibrations of the azide groups of cluster **C4** and polymer-cluster conjugates **POL5** and **POL6** in ATR FTIR spectra after subtraction of the corresponding spectrum of water.

After conjugation of **C4** with the precursor **P5**, affording **POL5**, and further introduction of amine groups along the polymer backbone affording **POL6**, the asymmetric stretching band intensity of the azide groups greatly decreased (Figure 3, blue and red lines) due to newly formed covalent bond. As the bands' position remained in the same region, the peak area tool in the OMNIC software was used to compare their intensities in the spectra of **POL5** and **POL6** using **C4** band as a reference. After the conjugation reaction,  $9\% \pm 1\%$  of azide groups remained unreacted for **POL5**, and similar value was found for **POL6**. This assessment indicates that the click reaction was successful as majority of the azide groups reacted.

The zeta potential of **POL5** conjugate ( $-17$  mV) was similar to the respective cluster **C4** ( $-16$  mV). As mentioned above, negatively charged nanoparticles could exhibit unfavorable pharmacokinetic properties after the body injection. Therefore, to avoid such behavior, part of the DBCO groups of polymer precursor **P5** was reacted with 3-azido-1-propylamine prior to addition of cluster **C4** to compensate, at least partially, the negative zeta potential of the polymer-cluster conjugate. Such combinational approach provided the polymer precursor with 1.5 mol. % of amine groups along the polymer backbone and consequently polymer-cluster conjugate **POL6** with zeta potential adjusted to  $-7$  mV, which is much more suitable for future therapeutic application of the developed polymer-cluster conjugates. Both  $M_w$  and  $D_h$  values proved the formation of polymer-cluster conjugates. The  $M_w$  slightly increased for **POL5** and **POL6** ( $M_w \approx 49,500$  g mol $^{-1}$  and  $52,000$  g mol $^{-1}$ , respectively) when compared to their precursor **P5** ( $M_w \approx 40,000$  g mol $^{-1}$ ) upon introduction of Mo $_6$  clusters in the structure. The hydrodynamic size remains similar to that of the other complexes, thus most probably forming the unimolecular complexes presented with a single or low number of cluster molecules. For physico-chemical and photophysical characteristics of polymer-cluster constructs **POL1–POL6**, see Table 3.

Importantly, we can summarize that we have successfully designed and synthesized several polymer-cluster systems differing in their inner structure and mode of the polymer-cluster interaction or bonding.

### 3.3. Stability and Photophysical Properties of the Polymer-Cluster Constructs

We further evaluated the colloidal stability and photophysical properties of the polymer-cluster constructs in PBS, a biologically relevant medium. In the case of **POL1** and

**POL2**, formed by electrostatic interactions, the complexes were not stable in any manner as the electrostatic interactions were not strong enough to keep the polymer-cluster complexes stable. **POL1** and **POL2** complexes in PBS immediately formed huge aggregates, and their precipitation was observed quite rapidly after their dissolution. In the case of **POL3** and **POL4**, exploiting the hydrophobic interactions, a slightly better stability in PBS was observed. Nevertheless, aggregates were also formed, suggesting that the hydrophobic polymer-cluster interactions were disrupted in PBS. Consequently, it was not possible to properly perform DLS, SEC or luminescence spectroscopy studies in PBS for any of these non-covalent complexes.

In terms of photophysical properties, the constructs were first studied in deionized water, where they displayed the typical broad emission band of the Mo<sub>6</sub> clusters with maxima in the 685–697 nm range (Figure 4). The emissivity was high with luminescence quantum yield ranging from 0.16 for **POL1** to 0.49 for **POL4** in argon saturated water (see Table 3). The quenching of the emission by oxygen was efficient with a fraction of triplet states quenched by oxygen in an air saturated solution ( $F_T = 1 - \Phi_L(\text{air})/\Phi_L(\text{Ar})$ ) of approximately 0.8 for all constructs, indicating good accessibility of the clusters to dissolved oxygen. This feature suggests an effective production of O<sub>2</sub>(<sup>1</sup>Δ<sub>g</sub>) which is a major factor for a successful photodynamic treatment. Overall, the luminescent properties of the clusters were preserved upon association with their respective polymers.

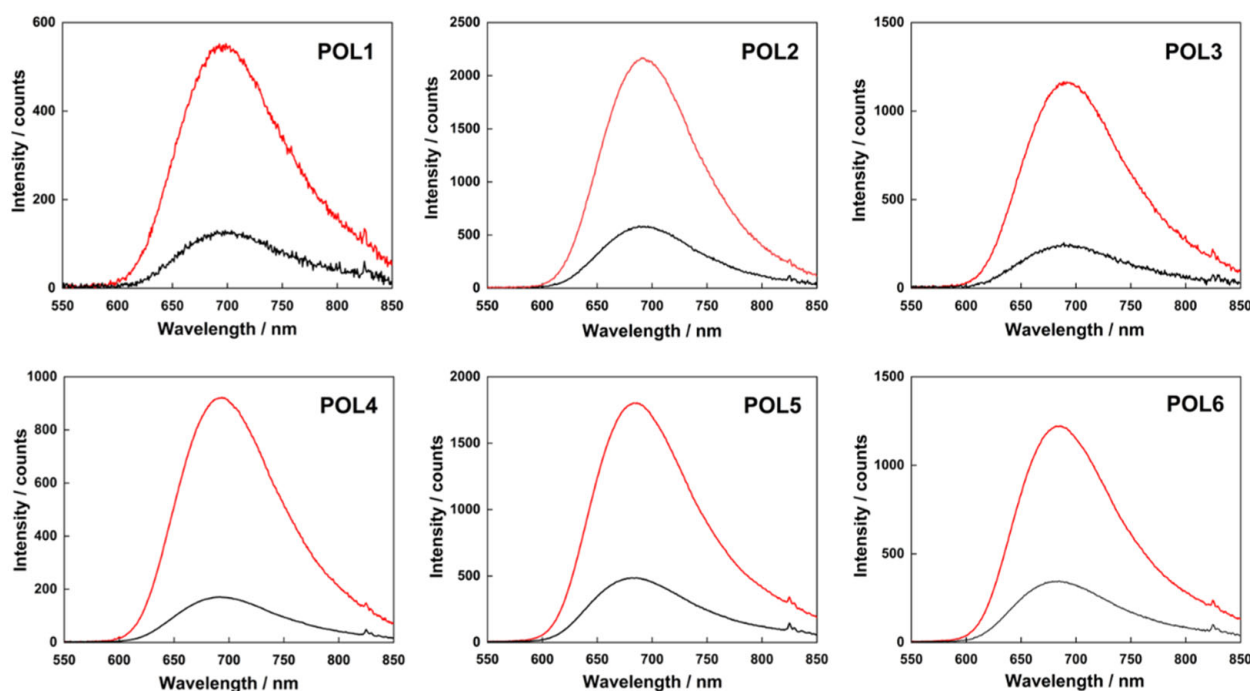


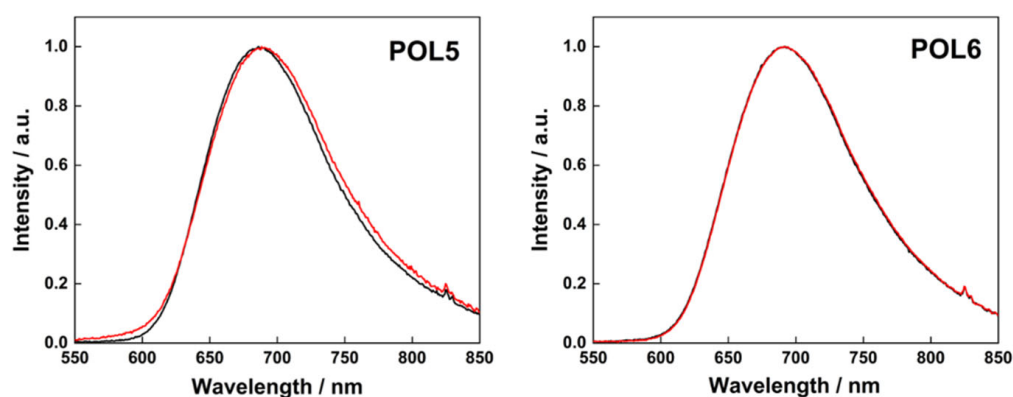
**Figure 4.** Luminescence emission spectra of **POL1**–**POL6** in deionized water: argon-saturated (red curve) and air-saturated (black curve) dispersions. All samples were excited at 400 nm.

In contrast to the non-covalent complexes which were not stable in PBS buffer, covalent polymer-cluster conjugates **POL5** and **POL6** displayed remarkable stability in PBS. Their hydrodynamic diameter of approximately 7–11 nm and ZP values did not change significantly even after 5 days (see Table 4). Additionally, no drastic changes were observed in the photophysical properties of the conjugates dissolved in PBS in comparison with deionized water solutions, except for slightly red shifted emission maxima and higher quantum yields (Table 4). The photophysical stability of the solutions was evaluated over a five-day period revealing no significant changes in the emission maxima, quantum yields, and oxygen quenching constant, which evidenced the high stability of the photosensitizing system (see Figure 5) in PBS. These features are attractive for photodynamic applications as a reasonable stability of the photosensitizing system is required for an effective PDT.

**Table 4.** Physico-chemical and photophysical characteristics of fresh solutions of polymer-cluster constructs in PBS and their stability after 5 days.

Polymer-Cluster Constructs	$D_H$ (nm) <sup>a</sup>	ZP (mV) <sup>a</sup>	$\lambda_L$ (nm) <sup>b</sup>	$\Phi_L(\text{Ar})$	$\Phi_L(\text{air})$	$F_T(\text{air})$
POL5, fresh	7.3 ± 1.1	−17	688	0.27	0.06	0.78
POL5, 5 days old	7.9 ± 1.4	−15	690	0.25	0.06	0.76
POL6, fresh	11.0 ± 0.9	−7	689	0.27	0.06	0.78
POL6, 5 days old	14.2 ± 0.1	−1	690	0.27	0.06	0.78

<sup>a</sup> The mean hydrodynamic diameter ( $D_H$ ) and zeta potential (ZP) were obtained by DLS with intensity of scattered light detected at angle  $\theta = 173^\circ$  in PBS. <sup>b</sup>  $\lambda_L$  is the maximum of luminescence emission bands;  $\Phi_L(\text{Ar})$  and  $\Phi_L(\text{air})$  are the luminescence quantum yields in argon- and air-saturated dispersions, respectively (excitation wavelength was 400 nm);  $F_T(\text{air})$  is the fraction of the triplet states quenched by oxygen in air saturated solutions:  $F_T(\text{air}) = 1 - \Phi_L(\text{air})/\Phi_L(\text{Ar})$ .

**Figure 5.** Normalized luminescence emission spectra of POL5 and POL6 in argon-saturated PBS. Solutions were fresh (black curve) or 5 days old (red curve). All samples were excited at 400 nm.

Taken all together, even though suitable photophysical properties were found for the polymer-cluster complexes, their colloidal stability in PBS does not allow further in vitro and in vivo testing and application. For polymer-cluster conjugates POL5 and POL6 bearing the Mo<sub>6</sub> cluster covalently bound to the polymer carrier, a very good stability and photophysical properties were observed. Both size and zeta potential were maintained after several days in PBS and even after months of storage as dried powders; hence, we believe that these conjugates are more suitable for further biomedical applications.

#### 4. Conclusions

This study described the design and synthesis of hydrophilic HPMA-based polymer constructs with Mo<sub>6</sub> clusters, potent singlet oxygen photosensitizers, and their structures' optimization from the chemical and physico-chemical point of view. We investigated three methods of preparation of the constructs using electrostatic, hydrophobic, or covalent interactions between the polymer backbone and cluster moieties. The luminescent properties of the Mo<sub>6</sub> clusters were preserved upon association with their respective polymers and all polymer-cluster constructs exhibited a production of O<sub>2</sub>(<sup>1</sup>Δ<sub>g</sub>), which is a major factor for a successful photodynamic treatment. The conjugates prepared by covalent interactions, such as the azide-alkyne “click chemistry”, were the best in the series—they possessed a high colloidal stability in PBS and provided high luminescence quantum yields. Moreover, a significant advantage of the synthesis is the fact that copper is completely avoided during the procedure. Results from physico-chemical and photophysical evaluation indicate that the conjugates with Mo<sub>6</sub> covalently attached to the polymer backbone are prospective candidates for biological evaluation including measurements of the cytotoxicity effect against selected cancer cells and in vivo experiments using suitable animal tumor models to assess the PDT efficacy of such system.

**Supplementary Materials:** The following supporting information can be downloaded at: <https://www.mdpi.com/article/10.3390/nano12193350/s1>, Detailed procedures for the synthesis of copolymer precursors and NMR spectra of selected precursors.

**Author Contributions:** M.R.T.—synthesis and characterization of copolymer precursors and polymer-cluster constructs, manuscript preparation and review; K.K.—synthesis and characterization of Mo<sub>6</sub> clusters, photoluminescence quantum yields measurements, manuscript review; N.K.—ATR FTIR measurements; M.P.—data analysis, manuscript review; K.L.—coordination of the project (Mo<sub>6</sub> cluster part), manuscript review; R.P.—synthesis of copolymer precursors and polymer-cluster constructs, manuscript preparation and review, corresponding author; T.E.—coordination of the project (polymer part), manuscript review. All authors have read and agreed to the published version of the manuscript.

**Funding:** We gratefully acknowledge the financial support from the Czech Science Foundation (grant No. 21-11688S) and the Ministry of Education, Youth and Sports of the Czech Republic within the Inter-excellence program (project LTAUSA18083).

**Data Availability Statement:** Not applicable.

**Acknowledgments:** The authors also acknowledge Petr Kašpárek for his excellent technical assistance and Rafał Łukasz Konefał for NMR measurements.

**Conflicts of Interest:** The authors declare no conflict of interest. The funders had no role in the design of the study; in the collection, analyses, or interpretation of data; in the writing of the manuscript; or in the decision to publish the results.

## References

1. Maeda, H.; Nakamura, H.; Fang, J. The EPR effect for macromolecular drug delivery to solid tumors: Improvement of tumor uptake, lowering of systemic toxicity, and distinct tumor imaging in vivo. *Adv. Drug Deliv. Rev.* **2013**, *65*, 71–79. [[CrossRef](#)] [[PubMed](#)]
2. Fang, J.; Šubr, V.; Islam, W.; Hackbarth, S.; Islam, R.; Etrych, T.; Ulbrich, K.; Maeda, H. N-(2-hydroxypropyl)methacrylamide polymer conjugated pyropheophorbide-a, a promising tumor-targeted theranostic probe for photodynamic therapy and imaging. *Eur. J. Pharm. Biopharm.* **2018**, *130*, 165–176. [[CrossRef](#)] [[PubMed](#)]
3. Berg, K.; Selbo, P.K.; Weyergang, A.; Dietze, A.; Prasmickaite, L.; Bonsted, A.; Engesaeter, B.Ø.; Angell-Petersen, E.; Warloe, T.; Frandsen, N.; et al. Porphyrin-related photosensitizers for cancer imaging and therapeutic applications. *J. Microsc.* **2005**, *218 Pt 2*, 133–147. [[CrossRef](#)]
4. Li, L.; Huh, K.M. Polymeric nanocarrier systems for photodynamic therapy. *Biomater. Res.* **2014**, *18*, 19. [[CrossRef](#)] [[PubMed](#)]
5. Chepurina, O.M.; Yakovliev, A.; Ziniuk, R.; Nikolaeva, O.A.; Levchenko, S.M.; Xu, H.; Losytsky, M.Y.; Bricks, J.L.; Slominskii, Y.L.; Vretik, L.O.; et al. Core-shell polymeric nanoparticles co-loaded with photosensitizer and organic dye for photodynamic therapy guided by fluorescence imaging in near and short-wave infrared spectral regions. *J. Nanobiotechnol.* **2020**, *18*, 19. [[CrossRef](#)] [[PubMed](#)]
6. Gibot, L.; Lemelle, A.; Till, U.; Moukarzel, B.; Mingotaud, A.-F.; Pimienta, V.; Saint-Aguet, P.; Rols, M.-P.; Gaucher, M.; Violleau, F.; et al. Polymeric Micelles Encapsulating Photosensitizer: Structure/Photodynamic Therapy Efficiency Relation. *Biomacromolecules* **2014**, *15*, 1443–1455. [[CrossRef](#)] [[PubMed](#)]
7. Lee, Y.-E.K.; Kopelman, R. Polymeric Nanoparticles for Photodynamic Therapy. In *Methods in Molecular Biology*; Springer: Clifton, NJ, USA, 2011; Volume 726, pp. 151–178.
8. Ricci-Júnior, E.; Marchetti, J.M. Preparation, characterization, photocytotoxicity assay of PLGA nanoparticles containing zinc (II) phthalocyanine for photodynamic therapy use. *J. Microencapsul.* **2006**, *23*, 523–538. [[CrossRef](#)]
9. Weiss, G.J.; Chao, J.; Neidhart, J.D.; Ramanathan, R.K.; Bassett, D.; Neidhart, J.A.; Choi, C.H.J.; Chow, W.; Chung, V.; Forman, S.J.; et al. First-in-human phase 1/2a trial of CRLX101, a cyclodextrin-containing polymer-camptothecin nanopharmaceutical in patients with advanced solid tumor malignancies. *Investig. New Drugs* **2013**, *31*, 986–1000. [[CrossRef](#)]
10. Brandhonneur, N.; Hatahet, T.; Amela-Cortes, M.; Molard, Y.; Cordier, S.; Dollo, G. Molybdenum cluster loaded PLGA nanoparticles: An innovative theranostic approach for the treatment of ovarian cancer. *Eur. J. Pharm. Biopharm.* **2018**, *125*, 95–105. [[CrossRef](#)]
11. Kiracki, K.; Demel, J.; Hynek, J.; Zelenka, J.; Rumlová, M.; Ruml, T.; Lang, K. Phosphinate Apical Ligands: A Route to a Water-Stable Octahedral Molybdenum Cluster Complex. *Inorg. Chem.* **2019**, *58*, 16546–16552. [[CrossRef](#)]
12. Kiracki, K.; Zelenka, J.; Rumlová, M.; Cvačka, J.; Ruml, T.; Lang, K. Cationic octahedral molybdenum cluster complexes functionalized with mitochondria-targeting ligands: Photodynamic anticancer and antibacterial activities. *Biomater. Sci.* **2019**, *7*, 1386–1392. [[CrossRef](#)] [[PubMed](#)]
13. Brandhonneur, N.; Boucaud, Y.; Verger, A.; Dumait, N.; Molard, Y.; Cordier, S.; Dollo, G. Molybdenum cluster loaded PLGA nanoparticles as efficient tools against epithelial ovarian cancer. *Int. J. Pharm.* **2021**, *592*, 120079. [[CrossRef](#)] [[PubMed](#)]

14. Smith, C.B.; Days, L.C.; Alajroush, D.R.; Faye, K.; Khodour, Y.; Beebe, S.J.; Holder, A.A. Photodynamic Therapy of Inorganic Complexes for the Treatment of Cancer<sup>†</sup>. *Photochem. Photobiol.* **2022**, *98*, 17–41. [[CrossRef](#)] [[PubMed](#)]
15. Kirakci, K.; Kubát, P.; Fejfarová, K.; Martinčík, J.; Nikl, M.; Lang, K. X-ray Inducible Luminescence and Singlet Oxygen Sensitization by an Octahedral Molybdenum Cluster Compound: A New Class of Nanoscintillators. *Inorg. Chem.* **2016**, *55*, 803–809. [[CrossRef](#)] [[PubMed](#)]
16. Kirakci, K.; Zelenka, J.; Rumlová, M.; Martinčík, J.; Nikl, M.; Ruml, T.; Lang, K. Octahedral molybdenum clusters as radiosensitizers for X-ray induced photodynamic therapy. *J. Mater. Chem. B* **2018**, *6*, 4301–4307. [[CrossRef](#)] [[PubMed](#)]
17. Kirakci, K.; Pozmogova, T.N.; Protasevich, A.Y.; Vavilov, G.D.; Stass, D.V.; Shestopalov, M.A.; Lang, K. A water-soluble octahedral molybdenum cluster complex as a potential agent for X-ray induced photodynamic therapy. *Biomater. Sci.* **2021**, *9*, 2893–2902. [[CrossRef](#)] [[PubMed](#)]
18. Koncošová, M.; Rumlová, M.; Mikyšková, R.; Reiniš, M.; Zelenka, J.; Ruml, T.; Kirakci, K.; Lang, K. Avenue to X-ray-induced photodynamic therapy of prostatic carcinoma with octahedral molybdenum cluster nanoparticles. *J. Mater. Chem. B* **2022**, *10*, 3303–3310. [[CrossRef](#)]
19. Felip-León, C.; Arnau del Valle, C.; Pérez-Laguna, V.; Isabel Millán-Lou, M.; Miravet, J.F.; Mikhailov, M.; Sokolov, M.N.; Rezusta-López, A.; Galindo, F. Superior performance of macroporous over gel type polystyrene as a support for the development of photo-bactericidal materials. *J. Mater. Chem. B* **2017**, *5*, 6058–6064. [[CrossRef](#)]
20. Vorotnikova, N.A.; Alekseev, A.Y.; Vorotnikov, Y.A.; Evtushok, D.V.; Molard, Y.; Amela-Cortes, M.; Cordier, S.; Smolentsev, A.I.; Burton, C.G.; Kozhin, P.M.; et al. Octahedral molybdenum cluster as a photoactive antimicrobial additive to a fluoroplastic. *Mater. Sci. Eng. C* **2019**, *105*, 110150. [[CrossRef](#)] [[PubMed](#)]
21. Kirakci, K.; Nguyen, T.K.N.; Grasset, F.; Uchikoshi, T.; Zelenka, J.; Kubát, P.; Ruml, T.; Lang, K. Electrophoretically Deposited Layers of Octahedral Molybdenum Cluster Complexes: A Promising Coating for Mitigation of Pathogenic Bacterial Biofilms under Blue Light. *ACS Appl. Mater. Interfaces* **2020**, *12*, 52492–52499. [[CrossRef](#)]
22. López-López, N.; Muñoz Resta, I.; de Llanos, R.; Miravet, J.F.; Mikhaylov, M.; Sokolov, M.N.; Ballesta, S.; García-Luque, I.; Galindo, F. Photodynamic Inactivation of Staphylococcus aureus Biofilms Using a Hexanuclear Molybdenum Complex Embedded in Transparent polyHEMA Hydrogels. *ACS Biomater. Sci. Eng.* **2020**, *6*, 6995–7003. [[CrossRef](#)] [[PubMed](#)]
23. Jackson, J.A.; Turro, C.; Newsham, M.D.; Nocera, D.G. Oxygen quenching of electronically excited hexanuclear molybdenum and tungsten halide clusters. *J. Phys. Chem.* **1990**, *94*, 4500–4507. [[CrossRef](#)]
24. Kirakci, K.; Kubát, P.; Langmaier, J.; Polívka, T.; Fuciman, M.; Fejfarová, K.; Lang, K. A comparative study of the redox and excited state properties of (nBu<sub>4</sub>N)<sub>2</sub>[Mo<sub>6</sub>X<sub>14</sub>] and (nBu<sub>4</sub>N)<sub>2</sub>[Mo<sub>6</sub>X<sub>8</sub>(CF<sub>3</sub>COO)<sub>6</sub>] (X = Cl, Br, or I). *Dalt. Trans.* **2013**, *42*, 7224. [[CrossRef](#)]
25. Kirakci, K.; Kubáňová, M.; Přibyl, T.; Rumlová, M.; Zelenka, J.; Ruml, T.; Lang, K. A Cell Membrane Targeting Molybdenum-Iodine Nanocluster: Rational Ligand Design toward Enhanced Photodynamic Activity. *Inorg. Chem.* **2022**, *61*, 5076–5083. [[CrossRef](#)] [[PubMed](#)]
26. Aubert, T.; Burel, A.; Esnault, M.A.; Cordier, S.; Grasset, F.; Cabello-Hurtado, F. Root uptake and phytotoxicity of nanosized molybdenum octahedral clusters. *J. Hazard. Mater.* **2012**, *219–220*, 111–118. [[CrossRef](#)]
27. Nakamura, H.; Liao, L.; Hitaka, Y.; Tsukigawa, K.; Subr, V.; Fang, J.; Ulbrich, K.; Maeda, H. Micelles of zinc protoporphyrin conjugated to N-(2-hydroxypropyl)methacrylamide (HPMA) copolymer for imaging and light-induced antitumor effects in vivo. *J. Control. Release* **2013**, *165*, 191–198. [[CrossRef](#)]
28. Ulbrich, K.; Subr, V.; Strohalm, J.; Plocová, D.; Jelínková, M.; Říhová, B. Polymeric drugs based on conjugates of synthetic and natural macromolecules. I. Synthesis and physico-chemical characterisation. *J. Control. Release* **2000**, *64*, 63–79. [[CrossRef](#)]
29. Šubr, V.; Ulbrich, K. Synthesis and properties of new N-(2-hydroxypropyl)-methacrylamide copolymers containing thiazolidine-2-thione reactive groups. *React. Funct. Polym.* **2006**, *66*, 1525–1538. [[CrossRef](#)]
30. Chytil, P.; Etrych, T.; Koňák, Č.; Šírová, M.; Mrkvan, T.; Bouček, J.; Říhová, B.; Ulbrich, K. New HPMA copolymer-based drug carriers with covalently bound hydrophobic substituents for solid tumour targeting. *J. Control. Release* **2008**, *127*, 121–130. [[CrossRef](#)]
31. Bojarová, P.; Tavares, M.R.; Laaf, D.; Bumba, L.; Petrásková, L.; Konefať, R.; Bláhová, M.; Pelantová, H.; Elling, L.; Etrych, T.; et al. Biocompatible glyconanomaterials based on HPMA-copolymer for specific targeting of galectin-3. *J. Nanobiotechnol.* **2018**, *16*, 73. [[CrossRef](#)]
32. Chytil, P.; Etrych, T.; Kříž, J.; Subr, V.; Ulbrich, K. N-(2-Hydroxypropyl)methacrylamide-based polymer conjugates with pH-controlled activation of doxorubicin for cell-specific or passive tumour targeting. Synthesis by RAFT polymerisation and physicochemical characterisation. *Eur. J. Pharm. Sci.* **2010**, *41*, 473–482. [[CrossRef](#)] [[PubMed](#)]
33. Perrier, S.; Takolpuckdee, P.; Mars, C.A. Reversible Addition–Fragmentation Chain Transfer Polymerization: End Group Modification for Functionalized Polymers and Chain Transfer Agent Recovery. *Macromolecules* **2005**, *38*, 2033–2036. [[CrossRef](#)]
34. Machová, D.; Koziolová, E.; Chytil, P.; Venclíková, K.; Etrych, T.; Janoušková, O. Nanotherapeutics with suitable properties for advanced anticancer therapy based on HPMA copolymer-bound ritonavir via pH-sensitive spacers. *Eur. J. Pharm. Biopharm.* **2018**, *131*, 141–150. [[CrossRef](#)]
35. Kirakci, K.; Zelenka, J.; Křížová, I.; Ruml, T.; Lang, K. Octahedral Molybdenum Cluster Complexes with Optimized Properties for Photodynamic Applications. *Inorg. Chem.* **2020**, *59*, 9287–9293. [[CrossRef](#)] [[PubMed](#)]

36. Kirakci, K.; Kubát, P.; Kučeráková, M.; Šícha, V.; Gbelcová, H.; Lovecká, P.; Grznárová, P.; Ruml, T.; Lang, K. Water-soluble octahedral molybdenum cluster compounds  $\text{Na}_2[\text{Mo}_6\text{I}_8(\text{N}_3)_6]$  and  $\text{Na}_2[\text{Mo}_6\text{I}_8(\text{NCS})_6]$ : Syntheses, luminescence, and in vitro studies. *Inorganica Chim. Acta* **2016**, *441*, 42–49. [[CrossRef](#)]
37. Etrych, T.; Mrkvan, T.; Chytil, P.; Koňák, Č.; Říhová, B.; Ulbrich, K. N-(2-hydroxypropyl)methacrylamide-based polymer conjugates with pH-controlled activation of doxorubicin. I. New synthesis, physicochemical characterization and preliminary biological evaluation. *J. Appl. Polym. Sci.* **2008**, *109*, 3050–3061. [[CrossRef](#)]
38. Fang, J.; Islam, W.; Maeda, H. Exploiting the dynamics of the EPR effect and strategies to improve the therapeutic effects of nanomedicines by using EPR effect enhancers. *Adv. Drug Deliv. Rev.* **2020**, *157*, 142–160. [[CrossRef](#)]
39. Pola, R.; Braunová, A.; Laga, R.; Pechar, M.; Ulbrich, K. Click chemistry as a powerful and chemoselective tool for the attachment of targeting ligands to polymer drug carriers. *Polym. Chem.* **2014**, *5*, 1340–1350. [[CrossRef](#)]
40. Filippov, S.K.; Chytil, P.; Konarev, P.V.; Dyakonova, M.; Papadakis, C.; Zhigunov, A.; Plestil, J.; Stepanek, P.; Etrych, T.; Ulbrich, K.; et al. Macromolecular HPMA-based nanoparticles with cholesterol for solid-tumor targeting: Detailed study of the inner structure of a highly efficient drug delivery system. *Biomacromolecules* **2012**, *13*, 2594–2604. [[CrossRef](#)]
41. Chytil, P.; Etrych, T.; Kostka, L.; Ulbrich, K. Hydrolytically Degradable Polymer Micelles for Anticancer Drug Delivery to Solid Tumors. *Macromol. Chem. Phys.* **2012**, *213*, 858–867. [[CrossRef](#)]
42. Filippov, S.K.; Vishnevetskaya, N.S.; Niebuur, B.J.; Koziolová, E.; Lomkova, E.A.; Chytil, P.; Etrych, T.; Papadakis, C.M. Influence of molar mass, dispersity, and type and location of hydrophobic side chain moieties on the critical micellar concentration and stability of amphiphilic HPMA-based polymer drug carriers. *Colloid Polym. Sci.* **2017**, *295*, 1313–1325. [[CrossRef](#)]
43. Chytil, P.; Šírová, M.; Kudláčová, J.; Říhová, B.; Ulbrich, K.; Etrych, T. Bloodstream Stability Predetermines the Antitumor Efficacy of Micellar Polymer–Doxorubicin Drug Conjugates with pH-Triggered Drug Release. *Mol. Pharm.* **2018**, *15*, 3654–3663. [[CrossRef](#)] [[PubMed](#)]
44. Braunová, A.; Chytil, P.; Laga, R.; Šírová, M.; Machová, D.; Parnica, J.; Říhová, B.; Janoušková, O.; Etrych, T. Polymer nanomedicines based on micelle-forming amphiphilic or water-soluble polymer-doxorubicin conjugates: Comparative study of in vitro and in vivo properties related to the polymer carrier structure, composition, and hydrodynamic properties. *J. Control. Release* **2020**, *321*, 718–733. [[CrossRef](#)] [[PubMed](#)]
45. Lieber, E.; Rao, C.N.R.; Hoffman, C.W.W.; Chao, T.S. Infrared Spectra of Organic Azides. *Anal. Chem.* **1957**, *29*, 916–918. [[CrossRef](#)]
46. Agrell, I.; Klæboe, P.; Pettersson, B.; Svensson, S.; Koskikallio, J.; Kachi, S. The Infra-red Spectra of Some Inorganic Azide Compounds. *Acta Chem. Scand.* **1971**, *25*, 2965–2974. [[CrossRef](#)]
47. Diana, E.; Gatterer, K.; Kettle, S.F.A. The vibrational spectroscopy of the coordinated azide anion; A theoretical study. *Phys. Chem. Chem. Phys.* **2016**, *18*, 414–425. [[CrossRef](#)]
48. Gai, X.S.; Coutifaris, B.A.; Brewer, S.H.; Fenlon, E.E. A direct comparison of azide and nitrile vibrational probes. *Phys. Chem. Chem. Phys.* **2011**, *13*, 5926–5930. [[CrossRef](#)]